catalysts

MDPI

Article

Dehydrogenation of Isobutane with Carbon Dioxide over SBA-15-Supported Vanadium Oxide Catalysts

Chunling Wei [1,2], Fangqi Xue [1], Changxi Miao [2,*], Yinghong Yue [1], Weimin Yang [2], Weiming Hua [1,*] and Zi Gao [1]

[1] Shanghai Key Laboratory of Molecular Catalysis and Innovative Materials, Department of Chemistry, Fudan University, Shanghai 200433, China; weicl.sshy@sinopec.com (C.W.); xuefqfighting@163.com (F.X.); yhyue@fudan.edu.cn (Y.Y.); zigao@fuan.edu.cn (Z.G.)

[2] Shanghai Research Institute of Petrochemical Technology SINOPEC, Shanghai 201208, China; yangwm.sshy@sinopec.com

* Correspondence: miaocx.sshy@sinopec.com (C.M.); wmhua@fudan.edu.cn (W.H.); Tel.: +86-21-68462197-5329 (C.M.); +86-21-65642409 (W.H.)

Academic Editor: Xiao-Feng Wu
Received: 31 August 2016; Accepted: 25 October 2016; Published: 31 October 2016

Abstract: A series of vanadia catalysts supported on SBA-15 (V/SBA) with a vanadia (V) content ranging from 1% to 11% were prepared by an incipient wetness method. Their catalytic behavior in the dehydrogenation of isobutane to isobutene with CO_2 was examined. The catalysts were characterized by N_2 adsorption, X-ray diffraction (XRD), scanning electron microscopy (SEM), Raman spectroscopy, and temperature-programmed reduction (TPR). It was found that these catalysts were effective for the dehydrogenation reaction, and the catalytic activity is correlated with the amount of dispersed vanadium species on the SBA-15 support. The 7% V/SBA catalyst shows the highest activity, which gives 40.8% isobutane conversion and 84.8% isobutene selectivity. The SBA-15-supported vanadia exhibits higher isobutane conversion and isobutene selectivity than the MCM-41-supported one.

Keywords: dehydrogenation; isobutane; carbon dioxide; vanadia; SBA-15; supported catalyst

1. Introduction

Currently, isobutene is mainly used as a chemical building block to produce polyisobutene, methyl tert-butyl ether (MTBE), butyl rubber, and methyl acrylates. Naphtha steam cracking and fluidized catalytic cracking, which are two primary methods to obtain isobutene, cannot provide sufficient isobutene for the expanding market due to the increasing demand for isobutene. Therefore, the dehydrogenation of isobutane is becoming an important approach to produce isobutene [1]. Although the process of direct isobutane dehydrogenation to isobutene was applied commercially [2], there are still some problems, such as it being limited by thermodynamic equilibrium, high energy consumption, and serious deactivation of the catalyst. The oxidative dehydrogenation of isobutane using O_2 has attracted much attention [3–7] because it is not limited by thermodynamic equilibrium and the energy consumption is relatively low. However, the selectivity toward isobutene is lower owing to the deep oxidation of isobutene, thus resulting in lower isobutene yield. Sugiyama et al. [4] found that Cr-FSM-16 showed ca. 9% yield of isobutene. Ehiro et al. [5] reported that Cr-MCM-41 catalyst gave an isobutene yield of ca. 7%.

The utilization of carbon dioxide as a mild oxidant for the selective dehydrogenation of small alkanes to their respective alkenes has gained much interest in recent years and is believed to be an attractive alternative to the traditional dehydrogenation [8–15]. Deep oxidation of the desirable dehydrogenation product to CO and CO_2 can be avoided via employing CO_2 instead of O_2. Hot sports can also be avoided due to the high heat capacity of CO_2. On the other hand, the use of CO_2 in the feed

also opens a new attractive pathway for CO_2 utilization, because in this new process it is reduced to CO which is more valuable in chemical industry. Attempts have been made for the dehydrogenation of isobutane to isobutene in the presence of CO_2. It is less extensively studied in comparison to the CO_2-assisted dehydrogenation of ethane and propane. The catalysts reported for this reaction mainly consist of iron oxide [16], vanadium–magnesium oxide [17], V_2O_5 [18], LaBaSm oxide [19], and NiO [15]. There is still a challenge in enhancing the catalytic activity and selectivity. The objective of the present study is to prepare mesoporous silica supported vanadia catalysts with superior catalytic performance. A vanadia catalyst supported on a mesoporous silica such as MCM-41 and SBA-15 exhibited good performance for the dehydrogenation of ethylbenzene with CO_2 [20–23]. Following this observation, in the present work, VO_x/SBA-15 catalysts were prepared by using mesoporous SBA-15 as the support. Their catalytic behavior in isobutane dehydrogenation with CO_2 has been studied, and compared with VO_x/MCM-41. The catalytic performance was correlated with the characterization results.

2. Results and Discussion

2.1. Characterization of Catalysts

As shown in Figure 1a, the parent SBA-15 shows an intense (100) diffraction peak and two other weaker peaks assigned to (110) and (200) reflections, suggesting that SBA-15 possesses ordered hexagonal mesostructure. This is consistent with the reported results [24,25]. A decrease in the intensity of the main (100) peak with an increase in vanadium content is observed, which may be caused by a partial degradation of the hexagonal arrangement of SBA-15 pores [26]. Nevertheless, three clear diffraction peaks still occurred for the SBA-15-supported samples at a V content of up to 7%, implying that the SBA-15 framework is well retained upon supporting vanadia. As the vanadium content increases to 11%, the (110) and (200) peaks become obscure, but the (100) peak can be clearly observed. This finding is indicative of a relatively severe collapse of the SBA-15 structure for the 11% V/SBA-15 sample. Figure 1b depicts the XRD patterns of the V/SBA samples with various V content in the wide-angle region. No diffraction peaks assigned to vanadium oxides appeared in the V/SBA catalysts with a V content of up to 3%, suggesting that the vanadium species in these samples are highly dispersed on the SBA-15 surface. With the increment of V content to 5%, weak diffraction peaks corresponding to crystalline V_2O_5 occurred, suggesting that bulk vanadia are formed at a high V content. A further increase in the V content on the SBA-15 support brings about an increment in the peak intensity. In contrast, the 7% V/MCM catalyst exhibits a similar XRD pattern to that of 7% V/SBA.

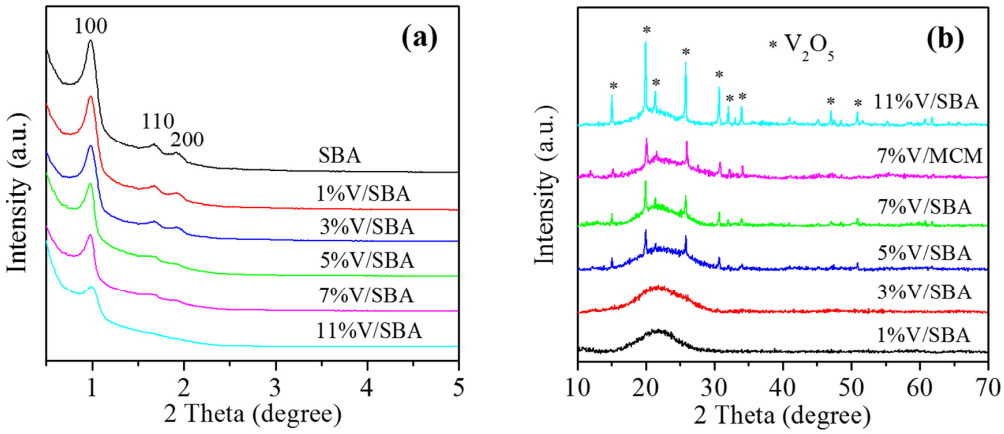

Figure 1. X-ray diffraction (XRD) patterns of SBA-15-supported vanadia catalysts in the small-angle region (**a**) and in the wide-angle region (**b**).

As shown in Figure 2, all SBA-15-supported vanadia catalysts possess type IV adsorption isotherms and type H1 hysteresis loops. A sharp inflection is found on the isotherms of V/SBA catalysts at P/P_o in the range of 0.6 and 0.75, implying that these materials have typical mesostructures. The textural properties of SBA-15-supported vanadia catalysts are listed in Table 1. As the V content increases, the surface area and pore volume of the V/SBA-15 samples decrease gradually. A high surface area and pore volume are observed in the SBA-15-supported samples with a V loading of up to 7%, which is indicative of the preservation of the SBA-15 framework. The significant decrease in surface area for the 11% V/SBA-15 sample as compared with that of the parent SBA-15 (555 m^2/g) is related to the relatively severe destruction of the SBA-15 framework. This is in agreement with the XRD results (Figure 1a).

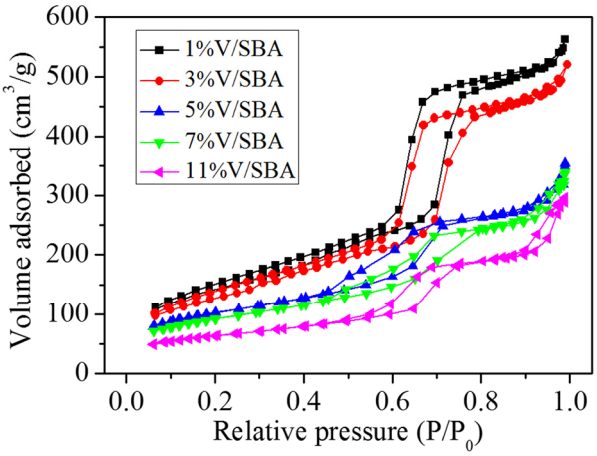

Figure 2. Nitrogen sorption isotherms of vanadia catalysts supported on SBA-15 (V/SBA) catalysts with different vanadium content.

Table 1. Physico-chemical properties of SBA-15-supported vanadia catalysts.

Catalyst	S_{BET} (m^2/g)	V_t [a] (cm^3/g)	D [b] (nm)	TPR Results [c]				AOS	NH_3-TPD Results [d]	
				T_M (°C)		H_2 Uptake (mmol/g)			T_M	Acidity
				I	II	I	II		(°C)	(mmol/g)
1% V/SBA	511	0.870	6.66	483	–	0.0618	–	4.4	192	0.030
3% V/SBA	458	0.805	6.64	489	577	0.279	0.0681	3.8	193	0.074
5% V/SBA	369	0.573	6.60	495	569	0.410	0.371	3.4	192	0.108
7% V/SBA	331	0.548	6.57	473	573	0.619	0.480	3.4	184	0.112
11% V/SBA	228	0.470	6.41	497	567	0.589	1.189	3.3	191	0.118
7% V/MCM	530	0.553	3.07	499	570	0.559	0.598	3.3	189	0.143

[a] Total pore volume; [b] Pore diameter at the maximum of the pore size distribution; [c] Peak temperature (T_M), H_2 consumption in mmol H_2/g of catalyst, and the average oxidation state (AOS) after TPR (temperature-programmed reduction) measurements; [d] Peak temperature (T_M), and the number of acid sites in mmol/g of catalyst.

Figure 3 displays the SEM images of 3% V/SBA and 7% V/SBA samples. The particles show rod-like morphology with the length of ca. 1 µm. The homogeneous distribution of V on both the 3% V/SBA and 7% V/SBA samples is shown by SEM-EDX mapping (Figure 4). Supplementary Materials Figure S1 presents the dark-field TEM images of 3% V/SBA and 7% V/SBA samples. Vanadium species cannot be found in the mesopores. We think that all the vanadium species are outside the mesopores.

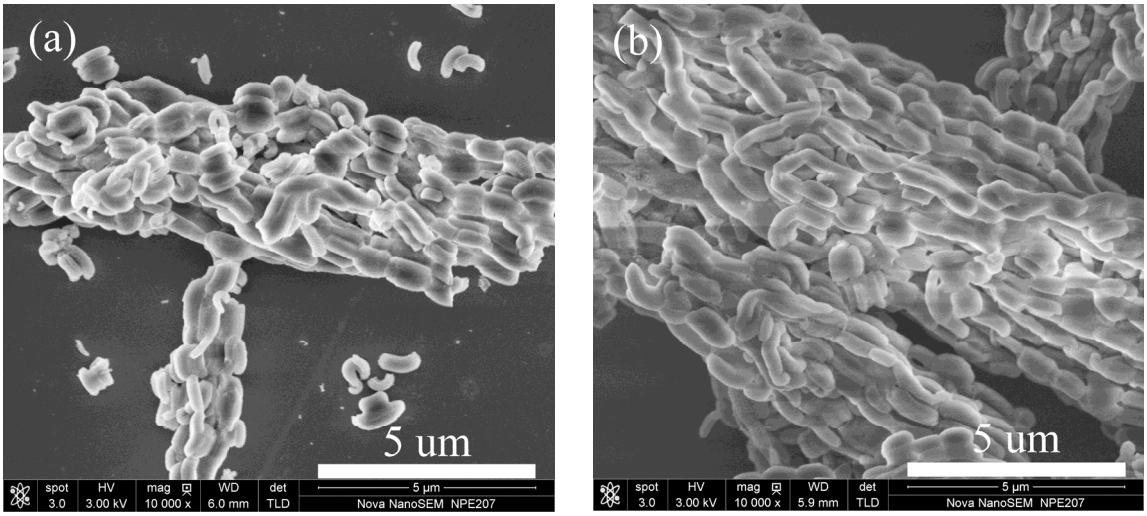

Figure 3. SEM images of (**a**) 3% V/SBA and (**b**) 7% V/SBA.

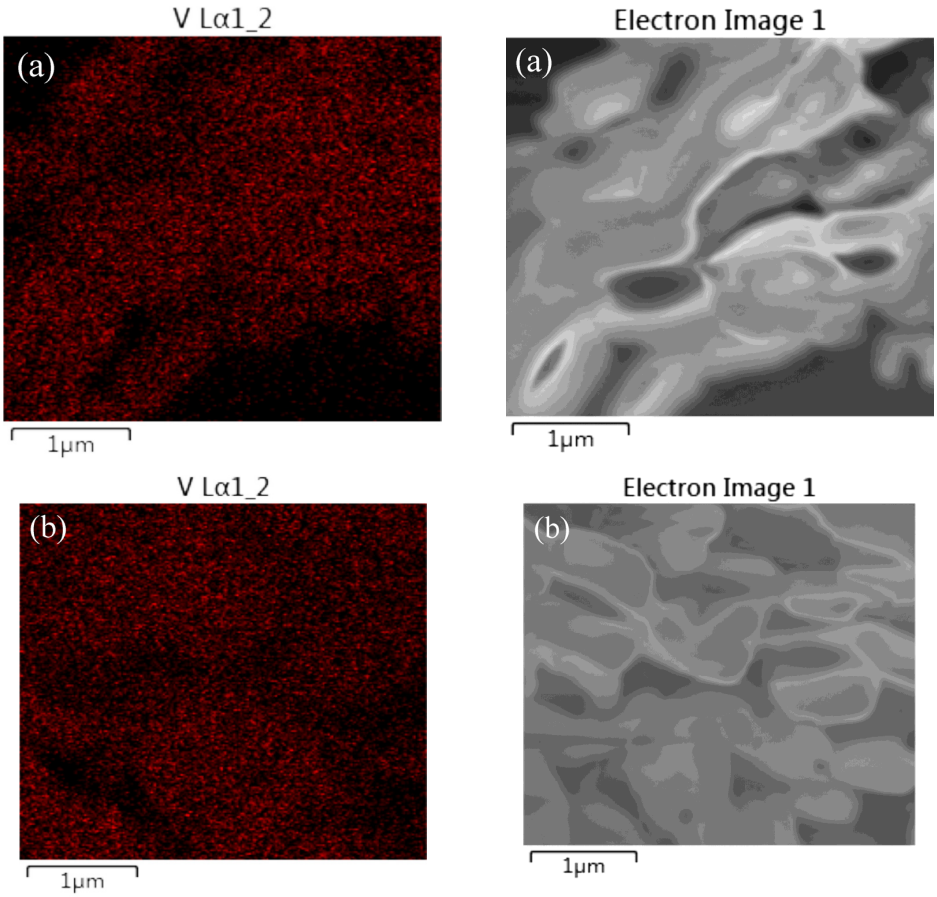

Figure 4. EDX elemental mapping of vanadia (V) (left column) and corresponding SEM images (right column) of (**a**) 3% V/SBA and (**b**) 7% V/SBA.

To reveal the molecular nature of the vanadium species dispersed on the SBA-15 support, Raman spectra of V/SBA samples with various V content are presented in Figure 5. The band at 1030 cm^{-1} is attributed to the symmetric stretching mode of the V=O bond in the isolated tetrahedral VO_4 species [27,28]. The band at 263 cm^{-1} can be ascribed to the V–O–V bending mode, and the bands at 420 and 512 may correlate with the V–O–V stretching vibrations [28]. The bands at 274, 402, 692,

and 990 cm^{-1} are characteristic of V_2O_5 crystallites [27,28]. The absence of a typical band at ca. 990 cm^{-1} of crystalline V_2O_5 in the 1% V/SBA sample suggests that crystallites of V_2O_5 are not formed. A shoulder band at 990 cm^{-1} is observed for the 3% V/SBA sample, suggesting that at a 3% V content, vanadium centers begin to aggregate to form V_2O_5 crystals. A close comparison of Figures 1b and 5 indicates that laser Raman spectroscopy is more sensitive than XRD for the identification of V_2O_5 crystallites in V/SBA samples. Other authors [27,29] also reported the same finding for the supported vanadia samples.

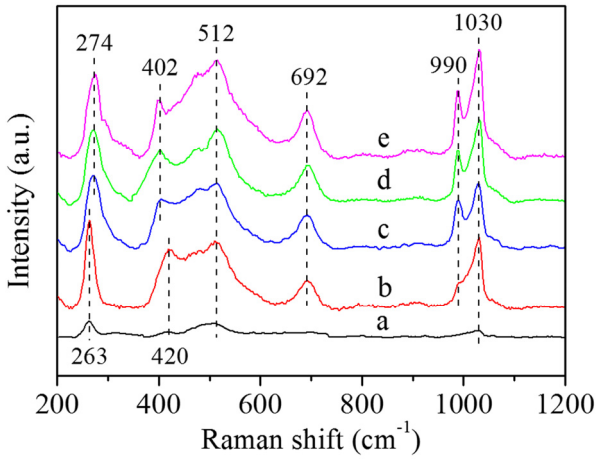

Figure 5. Raman spectra of V/SBA catalysts with different vanadium content. (**a**) 1% V/SBA; (**b**) 3% V/SBA; (**c**) 5% V/SBA; (**d**) 7% V/SBA; (**e**) 11% V/SBA.

Figure 6 presents the H_2-TPR profiles of the V/SBA samples with various V content obtained between 150 and 750 °C, and the H_2-TPR data are summarized in Table 1. For the sake of comparison, the profile and data of 7% V/MCM are also included. Only one reduction peak centered at 483 °C is observed on the V/SBA sample with a V content as low as 1%, corresponding to the reduction of V^{5+} [30–32]. At higher V content, there are two reduction peaks. The peak at low temperature (peak I) is attributed to the reduction of dispersed vanadium species, while the peak at high temperature (peak II) is assigned to the reduction of crystalline V_2O_5 [30,31]. The TPR results show that in addition to the dispersed vanadium species, large crystals of V_2O_5 exist on the V/SBA samples with a V content of 3% and above. This is consistent with the results of XRD and Raman measurements. The 7% V/SBA sample exhibits the lowest reduction temperature of peak I (473 °C), implying that this sample has the highest reducibility. As shown in Table 1, the amount of dispersed vanadium species increases with an increment in the V content from 1% to 7%. A further increase in the V content leads to a decrease in the amount of dispersed vanadium species. In contrast, a close comparison of the profiles for the 7% V/SBA and 7% V/MCM samples reveals that at the same V content level, the reduction peak temperature of peak I is lower for the SBA-15 catalyst than for that of its MCM-41 counterpart. This implies that the 7% V/SBA catalyst exhibits a higher reducibility than 7% V/MCM. Moreover, the former catalyst has more dispersed vanadium species than the latter one. After the H_2-TPR measurement, the 7% V/SBA sample was re-oxidized by 100% CO_2 at 570 °C for 0.5 h, then H_2-TPR was performed again. The H_2 consumption (0.439 mmol/g) is lower than that of the fresh catalyst (1.099 mmol/g), implying that CO_2 can act as a weak oxidant to oxidize the reduced vanadium species to a high oxidation state. However, the catalyst cannot be fully recovered to the original state.

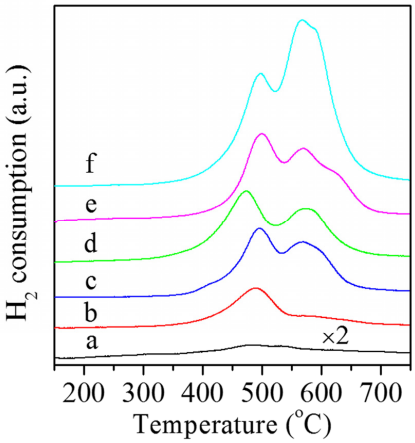

Figure 6. H_2-TPR (temperature-programmed reduction) profiles of V/SBA catalysts with different vanadium content. (**a**) 1% V/SBA; (**b**) 3% V/SBA; (**c**) 5% V/SBA; (**d**) 7% V/SBA; (**e**) 7% V/MCM; (**f**) 11% V/SBA.

On the other hand, in consideration of a total V^{5+}-to-V^{3+} reduction for every H_2 molecule consumed, the calculated average oxidation state (AOS) of vanadium after H_2 reduction [26] was listed in Table 1. The reduction of vanadium species happens from initial V^{5+} to V^{4+} and/or V^{3+} [30], but the final vanadium oxidation states depend on the V content. As shown in Table 1, the AOS of vanadium in the reduced catalysts decreases from 4.4 to 3.3 as the V loading increases from 1% to 11%. This suggests that bulk V_2O_5 could be reduced to a greater extent than the dispersed vanadium species [33].

Figure 7 shows the NH_3-TPD profiles of the V/SBA samples with various V content, and the data are listed in Table 1. The profile and data of 7% V/MCM are also included for comparision. All samples exhibit only one broad peak in the range of 120–350 °C, suggesting that the acid sites are of weak to medium strength. The peak temperature is similar, suggesting that acid strength is equivalent for these samples. The number of acid sites present on V/SBA-15 samples increases with the increment of V content from 1% to 5%, and increases slightly with the increment of V content from 5% to 11%. This result indicates that the acid sites presented over V/SBA-15 catalysts are associated with vanadia incorporation. The number of acid sites present on 7% V/SBA is 0.112 mmol/g, which is lower than that on 7% V/MCM (0.143 mmol/g).

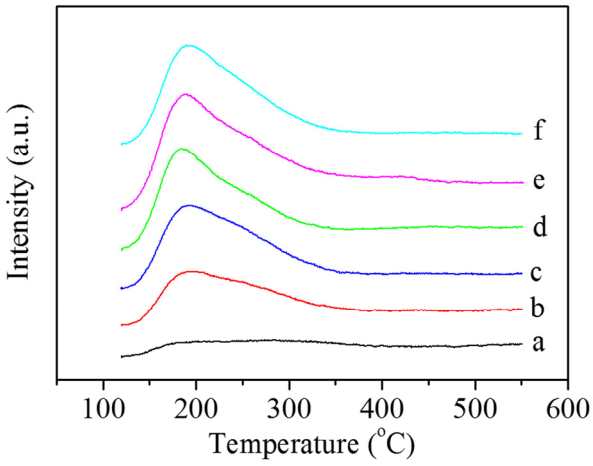

Figure 7. NH_3-TPD (temperature-programmed desorption) profiles of V/SBA catalysts with different vanadium content. (**a**) 1% V/SBA; (**b**) 3% V/SBA; (**c**) 5% V/SBA; (**d**) 7% V/SBA; (**e**) 7% V/MCM; (**f**) 11% V/SBA.

2.2. Catalytic Performance

The dehydrogenation of isobutane to isobutene in the presence of CO_2 over SBA-15-supported vanadia catalysts was investigated at 570 °C. The major hydrocarbon product formed in the reaction is isobutene, and the minor hydrocarbon products are methane, ethane, ethylene, propane, propylene, and butenes (except isobutene). Figure 8 depicts the catalytic performance of V/SBA catalysts with various V content as a function of reaction time. Isobutane conversion declines relatively quickly in the initial 30 min, followed by a slow decrease with reaction time, indicating a deactivation of the catalyst. Except that the 1% V/SBA catalyst exhibits almost a steady isobutene selectivity of ca. 90% during the reaction, the selectivity to isobutene for the other catalysts increases gradually, especially in the initial 90 min. This is due to a decrease in the amount of by-products, especially butenes (except isobutene). The results, shown in Figure 8, point to a marked composition effect on the catalytic performance of the V/SBA catalysts. Isobutane conversion initially increases with the increment of V content from 1% to 7%. A further increase in the V content results in a decline in conversion. The highest activity for isobutane dehydrogenation was achieved on the catalyst with a vanadium content of 7%, which demonstrates the superior performance of 7% V/SBA for the oxidative dehydrogenation of isobutane with CO_2. This catalyst gives a 40.8% conversion of isobutane with 84.8% selectivity to isobutene after 10 min on stream and a 23.1% conversion of isobutane with 89.1% selectivity to isobutene after 250 min on stream. Note that the blank test (without catalyst) shows isobutane conversion of ca. 2% under the same reaction conditions, suggesting that the contribution of the homogeneous reaction of isobutane is very small. Compared to isobutane conversion, the isobutene yield of V/SBA catalysts follows the same variation trend with V content, as shown in Table 2. The 7% V/SBA catalyst gives the highest isobutene yield. It is also seen in Table 2 that the more active catalyst for isobutane dehydrogenation with CO_2 has higher activity for CO_2 conversion to CO.

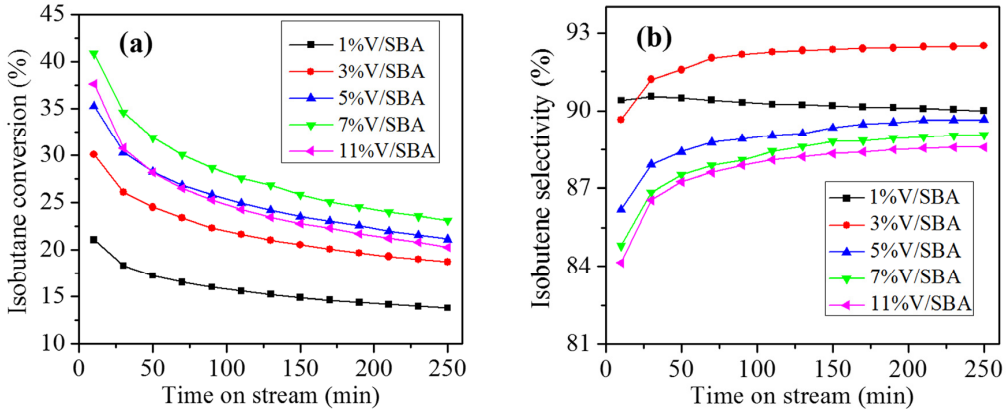

Figure 8. Conversion of isobutane (**a**) and selectivity to isobutene (**b**) as a function of time on stream for V/SBA catalysts at 570 °C.

Table 2. Reaction data of SBA-15-supported vanadia catalysts [a].

Catalyst	Conversion (%)		Selectivity (%)							i-C_4H_8
	i-C_4H_{10}	CO_2	i-C_4H_8	CH_4	C_2H_4	C_2H_6	C_3H_6	C_3H_8	C_4H_8 [b]	Yield (%)
1% V/SBA	21.1(13.8)	4.9(3.1)	90.4(90.0)	1.2(1.6)	0(0)	0(0)	3.1(4.2)	0.5(0.8)	4.8(3.4)	19.1(12.4)
3% V/SBA	30.0(18.7)	7.7(4.7)	89.7(92.5)	1.0(0.9)	0.2(0)	0.2(0)	2.2(2.3)	0.3(0.3)	6.4(4.0)	26.9(17.3)
5% V/SBA	35.2(21.9)	9.7(5.4)	86.2(89.7)	1.6(1.5)	0.3(0)	0.2(0)	3.2(3.8)	0.4(0.3)	8.1(4.7)	30.3(19.6)
7% V/SBA	40.8(23.1)	11.5(5.9)	84.8(89.1)	1.7(1.6)	0.3(0.2)	0.3(0)	3.5(3.9)	0.5(0.5)	8.9(4.7)	34.6(20.6)
11% V/SBA	37.6(20.3)	11.4(5.4)	84.2(88.6)	1.9(1.6)	0.3(0)	0.3(0)	3.6(4.1)	0.3(0.2)	9.4(5.5)	31.7(18.0)

[a] The values outside and inside the bracket are the data obtained at 10 min and 250 min, respectively; [b] Butenes except isobutene.

Supplementray Materials Figure S2 compares the catalytic performance of 7% V/SBA for isobutane dehydrogenation at 570 °C in the presence of CO_2 and in the absence of CO_2 (i.e., using N_2 instead of CO_2). The initial conversion of isobutane is higher in the presence of CO_2 than in the absence of CO_2. The selectivity to isobutene is higher in the presence of CO_2 than in the absence of CO_2. As far as the isobutene yield is concerned, it is greater in the presence of CO_2 than in the absence of CO_2 during 130 min of reaction, indicative of a promoting effect of CO_2 on the dehydrogenation of isobutane.

The redox behavior of vanadium oxide plays a key role in the dehydrogenation reaction using CO_2 as a mild oxidant over the vanadia-based catalysts. The easy redox cycle between fully oxidized and reduced vanadium species generates a highly active catalyst [31,34–37]. The variation of catalytic activity of V/SBA catalysts with vanadium content follows the same trend as the amount of dispersed vanadium species (Table 1), suggesting that the dispersed vanadium species on the SBA-15 support are mainly responsible for the catalytic activity in isobutane dehydrogenation with CO_2. This is reasonably understood, since dispersed vanadium species have higher reducibility and surface area than that of crystalline V_2O_5. The 7% V/SBA catalyst is the most active, which can be ascribed to the fact that this catalyst exhibits the highest reducibility and possesses the most dispersed vanadium species (Figure 6 and Table 1).

We compared the dehydrogenation of isobutane with CO_2 over vanadia catalysts supported on two different mesoporous silica (SBA-15 and MCM-41) at the same V content of 7%. The results, depicted in Figure 9, show that the activity of the 7% V/SBA catalyst is obviously higher than that of 7% V/MCM. Moreover, the former catalyst exhibits an evidently higher selectivity toward isobutene formation than the latter one. The 7% V/MCM catalyst only gives a 30.7% conversion of isobutane with 76.7% selectivity to isobutene after 10 min on stream and a 17.2% conversion of isobutane with 83.7% selectivity to isobutene after 250 min on stream. This finding suggests that, with a similar V content, SBA-15 is superior to MCM-41 as a support. From the H_2-TPR results, the higher catalytic activity of 7% V/SBA than 7% V/MCM is due to the fact that the former catalyst exhibits enhanced reducibility, as evidenced by the lower reduction temperature of peak I. Another reason is that the amount of dispersed vanadium species is greater for 7% V/SBA than 7% V/MCM. The higher isobutene selectivity achieved on 7% V/SBA than 7% V/MCM can be attributed to less acid sites present on the former catalyst, as indicated by the NH_3-TPD results. More acid sites favor the isomerization of isobutene to 1-butene and 2-butene, thus leading the diminishment of the selectivity toward isobutene.

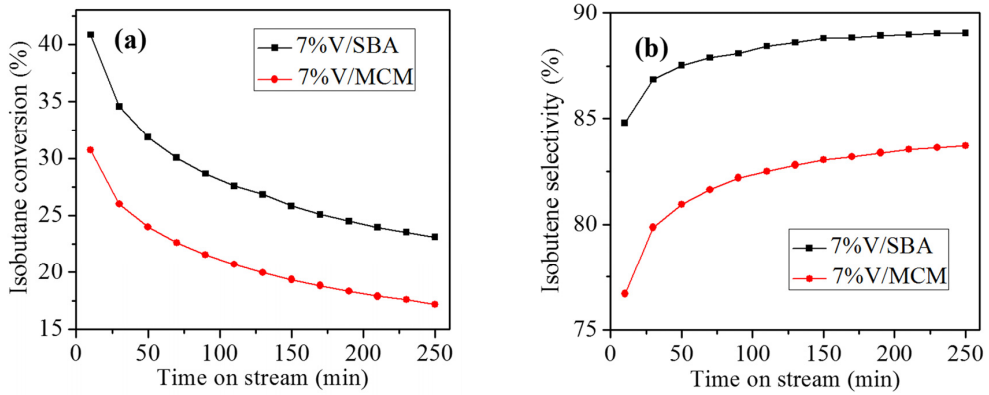

Figure 9. Conversion of isobutane (**a**) and selectivity to isobutene (**b**) as a function of time on stream for 7% V/SBA and 7% V/MCM catalysts at 570 °C.

It can be seen that the catalytic activity diminishes gradually with reaction time, as shown in Figure 8a. The colour of the catalysts becomes black after the dehydrogenation reaction, indicating the coke formation. The amount of coke deposited on the 7% V/SBA catalyst after 250 min of reaction, determined by TG, is 2.7%. The result, shown in Figure 10, clearly points to the production

of carbonaceous deposits on the spent 7% V/SBA catalyst. The G-band and D-band are observed at 1599 and 1340 cm^{-1}, respectively [38]. This result indicates the nature of the deposited carbon and reveals the graphitic and amorphous carbon deposition from isobutane dehydrogenation with CO_2. This observation indicates that the coke formation is mainly responsible for the deactivation of vanadia-based catalysts in dehydrogenation reactions in the presence of CO_2 [20,34,36,39].

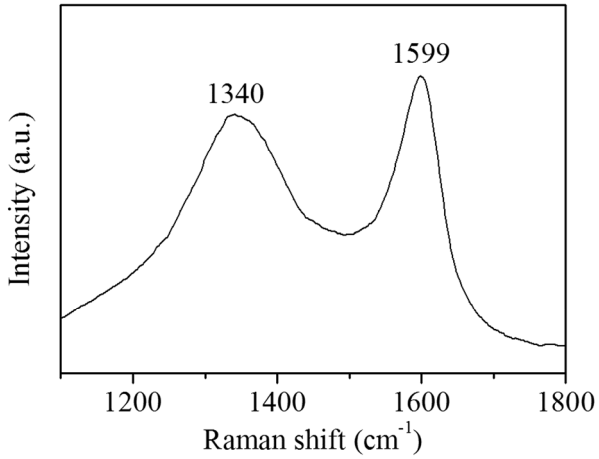

Figure 10. Raman spectrum of the spent 7% V/SBA catalyst after testing the dehydrogenation of isobutane with CO_2 at 570 °C for 250 min.

A regeneration treatment of the 7% V/SBA catalyst after 250 min of reaction at 570 °C in the presence of CO_2 was attempted. As shown in Figure 11, the isobutane conversion on 7% V/SBA decreases from 40.8% to 23.1% after 250 min on stream. The used catalyst was regenerated by re-calcination in flowing air at 550 °C for 2 h, followed by a purge with N_2 for another 1 h. The isobutane conversion on the regenerated catalyst is 38.5%, which is slightly lower than the initial conversion, indicating that the original activity of the catalyst can be almost completely restored. After the second and third regeneration, the activity of the catalyst is completely restored, which is caused by the removal of deposited carbon on the catalyst.

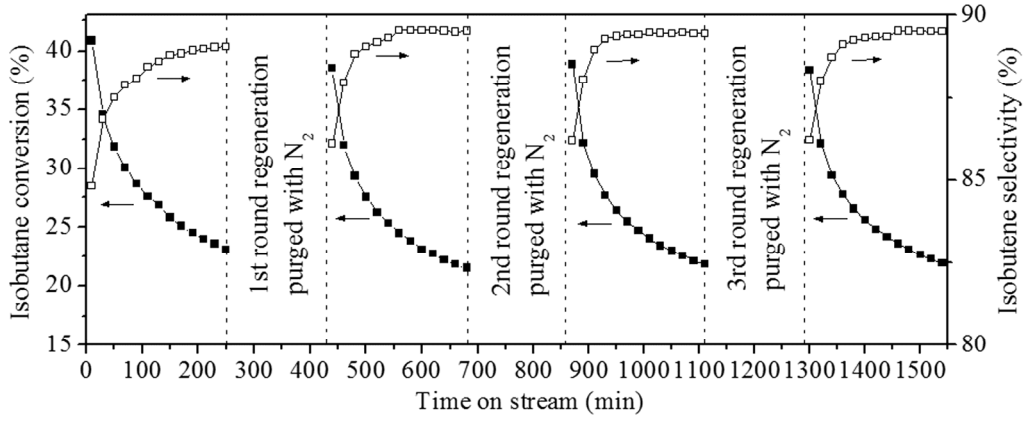

Figure 11. Regeneration of the 7% V/SBA catalyst at 550 °C. (■) conversion, (□) selectivity.

3. Materials and Methods

3.1. Catalyst Preparation

SBA-15 (BET surface area = 555 m^2/g, total pore volume = 0.875 cm^3/g) was obtained from Nanjing Pioneer Nanomaterials Science and Technology Co., Ltd. in Nanjing, China. The SBA-15-supported

vanadia catalysts were prepared by impregnating SBA-15 with a certain amount of NH_4VO_3 dissolved in an aqueous solution of oxalic acid (pH = ~1, NH_4VO_3/oxalic acid = 1/2 molar ratio). After impregnation, the catalysts were dried and calcined in static air at 600 °C for 4 h. The obtained catalysts are designated as *x*% V/SBA, where *x*% represents the wt % V in the catalysts. For comparison, a 7% V/MCM catalyst with a V content of 7% was prepared in the same way using mesoporous MCM-41 as a support. MCM-41 (BET surface area = 937 m^2/g, total pore volume = 0.979 cm^3/g) was available from the same company as SBA-15.

3.2. Catalyst Characterization

X-ray diffraction (XRD) patterns were collected on a MSAL XD2 X-ray diffractometer (PGENERAL, Beijing, China) using Cu Kα radiation at 40 kV and 30 mA. The BET specific surface areas and pore volumes of the catalysts were determined by the adsorption/desorption of nitrogen at liquid nitrogen temperature with a Micromeritics Tristar 3000 instrument (Micromeritics, Atlanta, GA, USA). The pore sizes of the catalysts were obtained from the peak positions of the distribution curves determined from the adsorption branches of the isotherms. Field-emission SEM images were recorded on Nova NanoSEM 450 (FEI, Hillsboro, TX, USA). TEM images were recorded on an FEI Tecnai G^2 F20 S-TWIN instrument (FEI, Hillsboro, TX, USA). Raman spectra were recorded on a HORIBA Jobin Yvon XploRA spectrometer (HORIBA Jobin Yvon, Paris, France). Wavelength of exciting light was selected as 532 nm.

Temperature-programmed reduction (TPR) profiles were obtained on a Micromeritics AutoChem II apparatus (Micromeritics, Atlanta, GA, USA) loaded with 100 mg of catalyst. The sample (40–60 mesh) was pretreated in flowing Ar at 300 °C for 3 h, and cooled to 150 °C in Ar. The sample was subsequently contacted with 10% H_2/Ar (30 mL/min), then heated, at a rate of 10 °C/min, to a final temperature of 750 °C. H_2 consumption was monitored using a thermal conductivity detector (TCD) (Micromeritics, Atlanta, GA, USA).

NH_3 temperature-programmed desorption (NH_3-TPD) experiments were conducted on a Micromeritics AutoChem II instrument with a TCD detector. Sample (0.15 g) (40–60 mesh) was pretreated in He flow at 550 °C for 1 h, and cooled to 120 °C. The flow was switched to 10% NH_3/He (30 mL/min) and kept for 2 h, and then swept by He (30 mL/min) for 2 h. Finally, the sample was heated in He (30 mL/min) to 550 °C at a rate of 10 °C/min.

3.3. Catalytic Tests

The oxidative dehydrogenation of isobutane with CO_2 was carried out in a homemade flow-type fixed-bed microreactor at 570 °C under atmospheric pressure. The catalyst (0.5 g) (40–60 mesh) was first pretreated at 570 °C in N_2 for 1 h. Then, a gas mixture of isobutane and CO_2 (1:5 molar ratio) flowed through the catalyst at a flow rate of 19.3 mL/min. The hydrocarbon products were analyzed using an on-line gas chromatograph (GC) (Agilent, Palo Alto, CA, USA) equipped with a flame ionization detector (Agilent, Palo Alto, CA, USA) and a HP-AL/S capillary column (50 m × 0.32 mm × 8.0 μm) (Agilent, Palo Alto, CA, USA). CO and CO_2 were analyzed on-line by another GC equipped with a TCD and a 6 m long stainless steel column packed with Porapak Q.

4. Conclusions

The SBA-15-supported vanadia catalysts (V/SBA) were prepared by the wet impregnation method. Textural and XRD results suggest that the ordered hexagonal mesostructure of the SBA-15 support is preserved after vanadium loading at least up to 7% V, and, therefore, high surface areas were obtained for the final catalysts. The V/SBA catalysts exhibit high activity for the dehydrogenation of isobutane to isobutene with CO_2, and the catalytic activity is correlated with the amount of dispersed vanadium species on the SBA-15 support. The 7% V/SBA catalyst shows the highest activity. An isobutane conversion of 40.8% with an isobutene selectivity of 84.8% was achieved using this catalyst at 570 °C and after reaction for 10 min. The higher catalytic activity observed for 7% V/SBA than for that of 7% V/MCM can be attributed to the enhanced reducibility and more dispersed vanadium species

on the former catalyst. The higher isobutene selectivity achieved on 7% V/SBA than for that on 7% V/MCM is due to the lower amount of acid sites on the former catalyst.

Supplementary Materials: The following are available online at www.mdpi.com/2073-4344/6/11/171/s1, Figure S1: High-angle annular dark field (HAADF) images of (**a**) 3% V/SBA and (**b**) 7% V/SBA, Figure S2: Catalytic performance of 7% V/SBA for isobutane dehydrogenation at 570 °C in the presence of CO_2 (■) and in the absence of CO_2 (●).

Acknowledgments: Weiming Hua thanks the Shanghai Research Institute of Petrochemical Technology SINOPEC (14ZC06070009) and the Science and Technology Commission of Shanghai Municipality (13DZ2275200) for financial support. Yinghong Yue thanks the National Natural Science Foundation of China (21273043) for financial support.

Author Contributions: C.M. and W.H. conceived and designed the experiments; C.W. and F.X. performed the experiments; Y.Y. and Z.G. analyzed the data; C.W. wrote the paper; W.H., C.M., and W.Y. revised the paper.

Conflicts of Interest: The authors declare no conflict of interest.

References

1. Sattler, J.J.H.B.; Ruiz-Martinez, J.; Santillan-Jimenez, E.; Weckhuysen, B.M. Catalytic dehydrogenation of light alkanes on metals and metal oxides. *Chem. Rev.* **2014**, *114*, 10613–10653. [CrossRef] [PubMed]
2. Resasco, D.E.; Marcus, B.K.; Huang, C.S.; Durante, V.A. Isobutane dehydrogenation over sulfided nickel catalysts. *J. Catal.* **1994**, *146*, 40–55. [CrossRef]
3. Neri, G.; Pistone, A.; De Rossi, S.; Rombi, E.; Milone, C.; Galvagno, S. Ca-doped chromium oxide catalysts supported on alumina for the oxidative dehydrogenation of isobutane. *Appl. Catal. A* **2004**, *260*, 75–86. [CrossRef]
4. Sugiyama, S.; Ehiro, T.; Nitta, Y.; Itagaki, A.; Nakagawa, K.; Katoh, M.; Katoh, Y.; Akihara, S.; Yasukawa, T.; Ninomiya, W. Acidic properties of various silica catalysts doped with chromium for the oxidative dehydrogenation of isobutane to isobutene. *J. Chem. Eng. Jpn.* **2015**, *48*, 133–140. [CrossRef]
5. Ehiro, T.; Itagaki, A.; Misu, H.; Kurashina, M.; Nakagawa, K.; Katoh, M.; Katou, Y.; Ninomiya, W.; Sugiyama, S. Oxidative dehydrogenation of isobutane to isobutene on metal-doped MCM-41 catalysts. *J. Chem. Eng. Jpn.* **2016**, *49*, 136–143. [CrossRef]
6. Al-zahrani, S.M.; Elbashir, N.O.; Abasaeed, A.E.; Abdulwahed, M. Isobutane oxydehydrogenation on Al_2O_3-supported transition and rare-earth metal oxides. *J. Mol. Catal. A* **2004**, *218*, 179–186. [CrossRef]
7. Cristina, R.; Zavoianu, R.; Portela, M. Isobutane oxydehydrogenation on SiO_2-supported nickel molybdate catalysts: Effect of the active phase loading. *Catal. Commun.* **2002**, *3*, 85–90.
8. Wang, S.B.; Zhu, Z.H. Catalytic conversion of alkanes to olefins by carbon dioxide oxidative dehydrogenation—A review. *Energy Fuels* **2004**, *18*, 1126–1139. [CrossRef]
9. Shi, X.J.; Ji, S.F.; Wang, K. Oxidative dehydrogenation of ethane to ethylene with carbon dioxide over Cr-Ce/SBA-15 catalysts. *Catal. Lett.* **2008**, *125*, 331–339. [CrossRef]
10. Takahara, I.; Chang, W.C.; Mimura, N.; Saito, M. Promoting effects of CO_2 on dehydrogenation of propane over a SiO_2-supported Cr_2O_3 catalyst. *Catal. Today* **1998**, *45*, 55–59. [CrossRef]
11. Wang, Y.; Ohishi, Y.; Shishido, T.; Zhang, Q.H.; Yang, W.; Guo, Q.; Wan, H.L.; Takehira, K. Characterizations and catalytic properties of Cr-MCM-41 prepared by direct hydrothermal synthesis and template-ion exchange. *J. Catal.* **2003**, *220*, 347–357. [CrossRef]
12. Shen, Z.H.; Liu, J.; Xu, H.L.; Yue, Y.H.; Hua, W.M.; Shen, W. Dehydrogenation of ethane to ethylene over a highly efficient Ga_2O_3/HZSM-5 catalyst in the presence of CO_2. *Appl. Catal. A Gen.* **2009**, *356*, 148–153. [CrossRef]
13. Michorczyk, P.; Ogonowski, J. Dehydrogenation of propane to propene over gallium oxide in the presence of CO_2. *Appl. Catal. A* **2003**, *251*, 425–433. [CrossRef]
14. Zheng, B.; Hua, W.M.; Yue, Y.H.; Gao, Z. Dehydrogenation of propane to propene over different polymorphs of gallium oxide. *J. Catal.* **2005**, *232*, 143–151. [CrossRef]
15. Ding, J.F.; Qin, Z.F.; Li, X.K.; Wang, G.F.; Wang, J.G. Catalytic dehydrogenation of isobutane in the presence of carbon dioxide over nickel supported on active carbon. *J. Mol. Catal. A* **2010**, *315*, 221–225. [CrossRef]

16. Shimada, H.; Akazawa, T.; Ikenaga, N.; Suzuki, T. Dehydrogenation of isobutane to isobutene with iron-loaded activated carbon catalyst. *Appl. Catal. A* **1998**, *168*, 243–250. [CrossRef]
17. Ogonowski, J.; Skrzńska, E. Activity of vanadium magnesium oxide supported catalysts in the dehydrogenation of isobutane. *Catal. Lett.* **2006**, *111*, 79–85. [CrossRef]
18. Nakagawa, K.; Kajita, C.; Ikenaga, N.; Ando, T.; Suzuki, T. Dehydrogenation of light alkanes over oxidized diamond-supported catalysts in the presence of carbon dioxide. *Catal. Today* **2003**, *84*, 149–157. [CrossRef]
19. Bi, Y.L.; Zhen, K.J.; Valenzuela, R.X.; Jia, M.J.; Corberán, V.C. Oxidative dehydrogenation of isobutane over LaBaSm oxide catalyst: Influence of the addition of CO_2 in the feed. *Catal. Today* **2000**, *61*, 369–375. [CrossRef]
20. Qiao, Y.Y.; Miao, C.X.; Yue, Y.H.; Xie, Z.K.; Yang, W.M.; Hua, W.M.; Gao, Z. Vanadium oxide supported on mesoporous MCM-41 as new catalysts for dehydrogenation of ethylbenzene with CO_2. *Microporous Mesoporous Mater.* **2009**, *119*, 150–157. [CrossRef]
21. Li, Z.H.; Su, K.M.; Cheng, B.W.; Shen, D.X.; Zhou, Y. Effects of VO_x/AlMCM-41 surface structure on ethylbenzene oxydehydrogenation in the presence of CO_2. *Catal. Lett.* **2010**, *135*, 135–140. [CrossRef]
22. Liu, B.S.; Rui, G.; Chang, R.Z.; Au, C.T. Dehydrogenation of ethylbenzene to styrene over $LaVO_x$/SBA-15 catalysts in the presence of carbon dioxide. *Appl. Catal. A* **2008**, *335*, 88–94. [CrossRef]
23. Liu, B.S.; Chang, R.Z.; Jiang, L.; Liu, W.; Au, C.T. Preparation and high performance of La_2O_3-V_2O_5/MCM-41 catalysts for ethylbenzene dehydrogenation in the presence of CO_2. *J. Phys. Chem. C* **2008**, *112*, 15490–15501. [CrossRef]
24. Zhao, D.; Feng, J.; Huo, Q.; Melossh, N.; Fredrickson, G.H.; Chmelka, B.F.; Stucky, G.D. Triblock copolymer syntheses of mesoporous silica with periodic 50 to 300 angstrom pores. *Science* **1998**, *279*, 548–552. [CrossRef] [PubMed]
25. Hua, W.M.; Yue, Y.H.; Gao, Z. Acidity enhancement of SBA mesoporous molecular sieve by modification with SO_4^{2-}/ZrO_2. *J. Mol. Catal. A* **2001**, *170*, 195–202. [CrossRef]
26. Liu, Y.M.; Cao, Y.; Yi, N.; Feng, W.L.; Dai, W.L.; Yan, S.R.; He, H.Y.; Fan, K.N. Vanadium oxide supported on mesoporous SBA-15 as highly selective catalysts in the oxidative dehydrogenation of propane. *J. Catal.* **2004**, *224*, 417–428. [CrossRef]
27. Khodakov, A.; Olthof, B.; Bell, A.T.; Iglesia, E. Structure and catalytic properties of supported vanadium oxides: Support effects on oxidative dehydrogenation reactions. *J. Catal.* **1999**, *181*, 205–216. [CrossRef]
28. Chao, K.J.; Wu, C.N.; Chang, H.; Lee, L.J.; Hu, S.F. Incorporation of vanadium in mesoporous MCM-41 and microporous AFI zeolites. *J. Phys. Chem. B* **1997**, *101*, 6341–6349. [CrossRef]
29. Liu, Y.; Cao, Y.; Yan, S.; Dai, W.; Fan, K. Highly effective oxidative dehydrogenation of propane over vanadia supported on mesoporous SBA-15 silica. *Catal. Lett.* **2003**, *88*, 61–67. [CrossRef]
30. Solsona, B.; Nieto, J.M.L.; Díaz, U. Siliceous ITQ-6: A new support for vanadia in the oxidative dehydrogenation of propane. *Microporous Mesoporous Mater.* **2006**, *94*, 339–347. [CrossRef]
31. Chen, S.; Qin, Z.; Xu, X.; Wang, J. Structure and properties of the alumina-supported vanadia catalysts for ethylbenzene dehydrogenation in the presence of carbon dioxide. *Appl. Catal. A* **2006**, *302*, 185–192. [CrossRef]
32. Dai, H.; Bell, A.T.; Iglesia, E. Effects of molybdena on the catalytic properties of vanadia domains supported on alumina for oxidative dehydrogenation of propane. *J. Catal.* **2004**, *221*, 491–499. [CrossRef]
33. Berndt, H.; Martin, A.; Brückner, A.; Schreier, E.; Müller, D.; Kosslick, H.; Wolf, G.U.; Lücke, B. Structure and catalytic properties of VO_x/MCM materials for the partial oxidation of methane to formaldehyde. *J. Catal.* **2000**, *191*, 384–400. [CrossRef]
34. Sakurai, Y.; Suzaki, T.; Nakagawa, K.; Ikenaga, N.; Aota, H.; Suzuki, T. Dehydrogenation of ethylbenzene over vanadium oxide-loaded MgO catalyst: Promoting effect of carbon dioxide. *J. Catal.* **2002**, *209*, 16–24. [CrossRef]
35. Chang, J.S.; Vislovskiy, V.P.; Park, M.S.; Hong, D.Y.; Yoo, J.S.; Park, S.E. Utilization of carbon dioxide as soft oxidant in the dehydrogenation of ethylbenzene over supported vanadium-antimony oxide catalyst. *Green Chem.* **2003**, *5*, 587–590. [CrossRef]
36. Yuan, R.X.; Li, Y.; Yan, H.B.; Wang, H.; Song, J.; Zhang, Z.S.; Fan, W.B.; Chen, J.G.; Liu, Z.W.; Liu, Z.T.; et al. Insights into the vanadia catalyzed oxidative dehydrogenation of isobutane with CO_2. *Chin. J. Catal.* **2014**, *35*, 1329–1336. [CrossRef]

37. Ascoop, I.; Galvita, V.V.; Alexopoulos, K.; Reyniers, M.F.; Van Der Voort, P.; Bliznuk, V.; Marin, G.B. The role of CO_2 in the dehydrogenation of propane over WO_x–VO_x/SiO_2. *J. Catal.* **2016**, *335*, 1–10. [CrossRef]
38. De Morais Batista, A.H.; Ramos, F.S.O.; Braga, T.P.; Lima, C.L.; de Sousa, F.F.; Barros, E.B.D.; Filho, J.M.; de Oliveira, A.S.; de Sousa, J.R.; Valentini, A.; et al. Mesoporous MAl_2O_4 (*M*=Cu, Ni, Fe or Mg) spinets: Characterisation and application in the catalytic dehydrogenation of ethylbenzene in the presence of CO_2. *Appl. Catal. A* **2010**, *382*, 148–157. [CrossRef]
39. Sun, A.L.; Qin, Z.F.; Chen, S.W.; Wang, J.G. Ethylbenzene dehydrogenation in the presence of carbon dioxide over alumina supported catalysts. *Catal. Today* **2004**, *93–95*, 273–279. [CrossRef]